DESIGN, CONSTRUCTION AND TESTING OF A FIVE ACTIVE AXES MAGNETIC BEARING SYSTEM

Cristiana Delprete, Giancarlo Genta
Dipartimento di Meccanica, Politecnico di Torino
Torino, Italy

Stefano Carabelli
Dipartimento di Automatica e Informatica, Politecnico di Torino
Torino, Italy

SUMMARY

A high speed electric spindle based on active electromagnetic suspension technology has been designed, built and tested. The main goal of the research work was the construction of a highly modular unit which can be used both for teaching and research purposes. The design of the electromechanical components and of the control unit is described in detail, together with the characterization tests performed on the various subsystems. A description of the preliminary tests on the unit, conducted at speeds not in excess of the first deformation critical speed of the rotor, concludes the work.

INTRODUCTION

After having gained experience in the design and construction of passive magnetic bearing systems [1], [2], [3], at the Department of Mechanics of Politecnico di Torino, the designand construction of a five-active axes magnetic suspension was undertaken. The prototype chosen was an electric spindle which could be operated in a wide range of speeds and operating conditions. Together with the aim of gaining a direct experience in the field, the goal was to build a prototype which could be used both for teaching and research purposes.

The following design requirements were stated: modularity of both the mechanical and the electronic layout; low weight for enhancing transportability; easy access to the various parts for introducing instrumentation and for maintenance; possibility of visual check of the various parts during operation; possibility of changing the configuration of the mechanical parts by shifting axially the subsystems and substituting the shaft; conformity with IEC 348 electrical safety standard; control unit with separate boards for each controlled axis; possibility of substituting each mechanical or electronic component and to use external digital or analogic controllers for any one of the axes.

Work sponsored by Italian Ministry of University and Scientific Research under the 40% and 60% research grants.

The present prototype has no aim of representing the optimum solution for any particular type of machine with magnetic suspension, neither for the electromechanical parts nor for the control architecture. The driving idea of the project is that of obtaining a flexible research tool for basic research in the field of magnetic bearings and their control systems, for testing new ideas and control strategies and finally for the development of practical design of components. The effects of different control architectures on the rigid-body or flexible-body dynamics of the system (SISO *PID*, Lead-Lag...) can be studied and different digital controllers (SISO and MIMO) can be compared. With some modifications the system can simulate the effects of the various controllers on machines with complex configuration such as gas turbines or turbomolecular pumps.

The device is also intended for teaching purposes, mainly to demonstrate the principles of active magnetic suspension to mechanical and electronic engineering students and to show them the effects of the various control parameters on the stability and the dynamic behaviour in general. By changing the values of the control parameters acting on the knobs of the control panel it is possible to demonstrate the effects of changes of the gains and time constants of the compensator on the dynamic behaviour of the rotor.

At present the research work is aimed to implementing various configurations of the compensator with the aim of controlling the first deformation mode of the rotor to operate at speeds higher than the corresponding critical speed; investigating modal control and automatic balancing strategies; developing and testing actuators biased by permanent magnets to reduce the power consumption, which is at any rate very low; and developing and testing digital controllers.

Wherever possible particular care was devoted to choose design alternatives leading to low-cost components, or, at least, components which could be produced at low cost if the unit had to be produced in a small quantity. Configurations which are standard in other types of electromechanical devices (e.g. electric motors) were used all where possible. As a result the cost of the whole research was very reasonable and the prototype can be produced in small quantities as a didactic and research rig at a very competitive cost.

The research and design work started with a survey of the literature existing on the subject. Since it is impossible to report a comprehensive bibliography here, a small number of papers are cited [4] - [10].

GENERAL LAYOUT

As already stated a modular design was chosen; the electro-mechanical subsystem consists of a shaft and five stator units which are bolted together, namely

- two radial bearing units which include the radial sensors and the emergency ball bearings;
- one axial bearing unit;
- one asynchronous a.c. electric motor unit;
- a base which includes the axial sensor and carries all electrical connectors and signal conditioners of the sensors.

The power unit is a solid-state frequency converter which can feed the electric motor with a 3-phase alternating voltage with controllable frequency in the 30-1000 Hz range. The maximum voltage at 1000 Hz is 90 V. The maximum power rating of the converter is 2 kW.

The controller unit contains the five independent controller boards, each one containing its power amplifier. Both the controller and the power unit are fed directly from the two-phase, 50 Hz, 220 V mains.

A picture of the system is shown in Figure 1.

Axial actuator

The axial bearing is made by two electromagnets housed in a light-alloy (Al SG91 UNI 7369/3) cast support. The magnetic circuit (C40 steel UNI 7845) is made in two parts, each one carrying an electromagnet; it closes through a disc (39NiCrMo3 steel UNI 7845 hardened and tempered) shrunk-fit on the shaft on which the electromagnetic axial force is exerted (Figure 2). The steel disc is the largest part of the rotor and is the most stressed by centrifugal loading; for this reason a steel which is more suitable for highly stressed applications than for magnetic circuits has been used. The stress field in the disc has been computed using a standard procedure for rotating discs; the maximum speed of the rotor has then been stated at a value of 35000 rpm, at which the maximum equivalent stress (Von Mises criterion) is 163 MN/m^2.

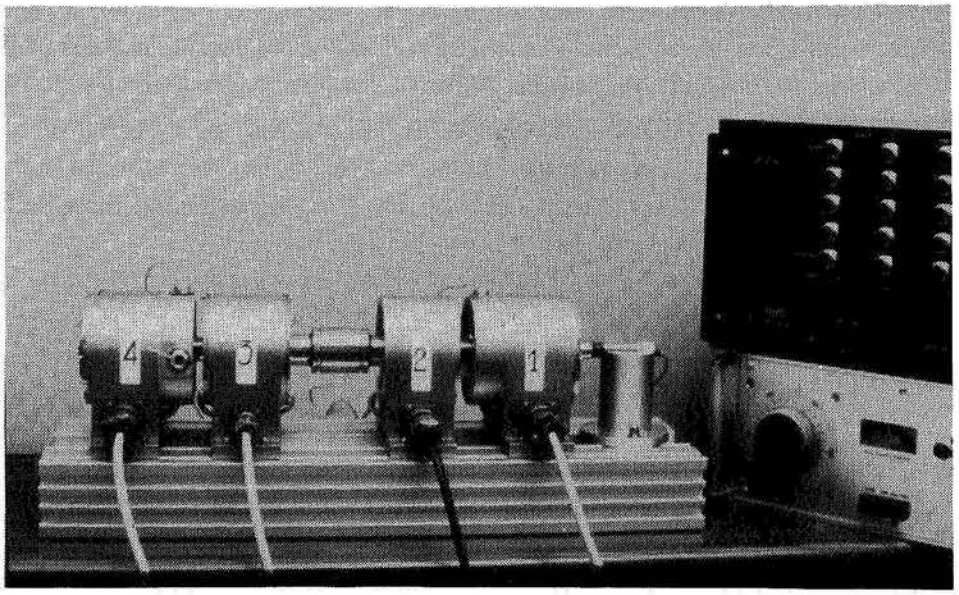

Figure 1. Picture of the complete system.
1: Radial actuator,
2: electric motor,
3: axial actuator,
4: Radial actuator.

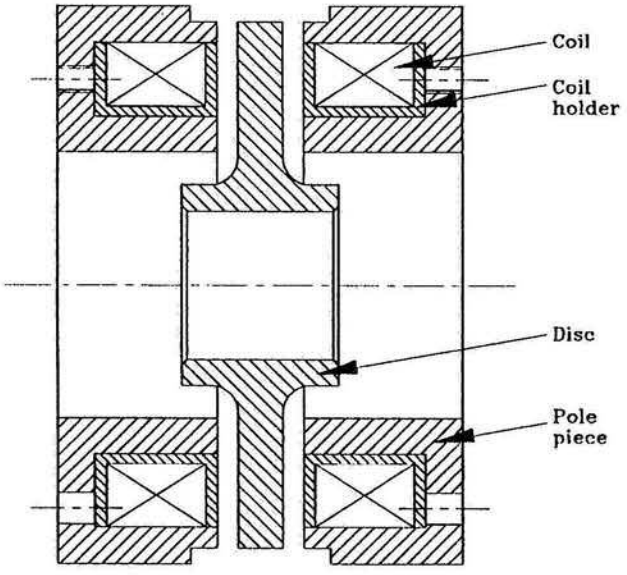

Figure 2. Magnetic circuit of the axial bearing (the air gap is not to scale).

The magnetic force was computed using a very simple model in which the material is assumed to have a linear magnetic behaviour (with $\mu_{Fe} = 1.6\ 10^{-3}$ H/m, equal to that of cast steel), no stray flux is accounted for, the reluctance of the iron parts is neglected if compared with that of the air gap and the flux is assumed to be constant on each area perpendicular to it. This model is adequate only for working conditions in which the magnetic circuit is far from saturation and the air gap is not too small and yields a value of the magnetic forces which is higher than the actual one.

By neglecting the reluctance of the pole pieces, the axial force, the resistance and inductance of the electromagnets are computed

$$F_{ax} = \frac{B_t^2 S_t}{2\mu_0} + \frac{B_{Fe}^2 S_{Fe}}{2\mu_{Fe}} \approx \mu_0 \frac{N^2 i^2}{4t^2} S_t \quad , \qquad R = \rho N \frac{l_{sm}}{S_f} \quad , \qquad L \approx \mu_0 \frac{N^2 S_t}{2t} \quad . \tag{1}$$

where B_t, B_{Fe}, μ_0, μ_{Fe}, S_t, S_{Fe}, N, i, l_{sm}, S_f and ρ are respectively the magnetic flux densities in the air gap and the pole pieces, the magnetic permeabilities of vacuum and the material, the cross sectional areas of the air gap and the magnetic circuit (assumed as constant), the number of turns, the current, the mean length of each turn, the cross section of the wire and the resistivity of copper. The nominal air gap is $t = 0.75$ mm.

For the coil 8 layers of 15 turns each ($N = 120$) of wire with a diameter of 1.3 mm was used. The current density at 10 A is $J = 6.8$ A/mm^2, within the allowable limits for copper. A maximum axial force of 243 N at 5 A with the nominal air gap of 0.75 mm is so computed.

Radial actuators

The two identical radial actuators are very similar to asynchronous squirrel cage a.c. motors, the differences mainly being in the different winding pattern and in the lack of the squirrel cage (copper conductors) in the laminations of the rotor (Figure 3). The actuators are housed in casings which are essentially equal to those of the axial bearing, being obtained from the same casting with some different machining. The rotoric and statoric magnetic circuits are obtained from 100 laminations of thin soft iron sheet (loss factor = 1.1 W/kg, $\mu_{Fe} = 5.7\ 10^{-3}$ H/m). 50 laminations are obtained from insulated sheets (thickness 0.43 mm) and 50 from noninsulated sheets (0.37 mm). The laminated structure is aimed to reduce losses due to eddy currents, as usual.

The magnetic circuit of the stator has eight slots and hence standard motor laminations cannot be used. As the number of layers is too low to justify the construction of a punch, they were obtained at a fairly low cost by chemical milling. The electromagnets are wound in such a way to obtain 4 horseshoe independent electromagnets at 90 degrees phasing.

The width of the pole pieces is $l = 12$ mm, giving way to an active surface $S_t = 444$ mm^2. The shape of the slots has been designed in such a way to avoid strong flux concentrations which could lead to saturated zones at high values of the current. A total of 110 turns of double wire of 0.9 mm diameter were wound. At a peak value of the current of 8 A, corresponding to 115% of the value which would cause the magnetic saturation of the soft iron pole pieces, the current density ($J = 6.4$ A/mm^2) is still acceptable.

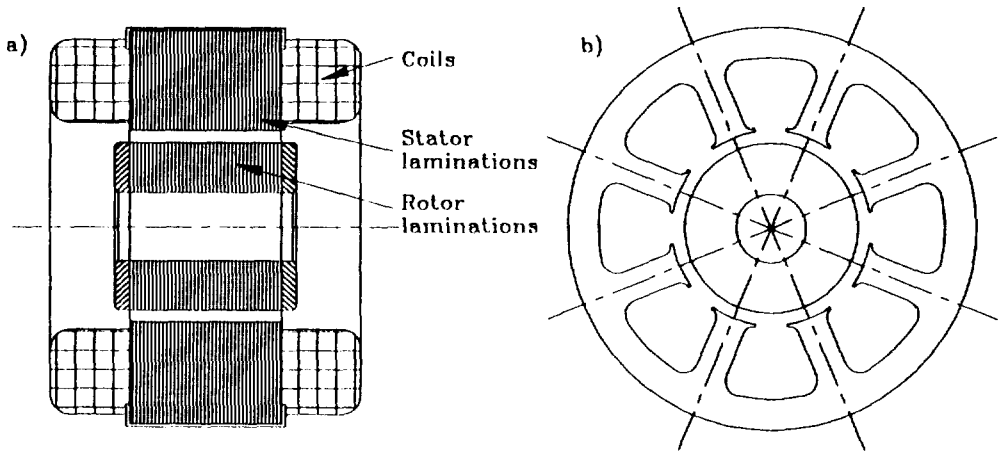

Figure 3. Radial bearing. a) Cross section of the magnetic circuit; b) shape of the rotor and stator laminations (the air gap is not to scale).

A first mathematical model which is essentially the same as that of the axial bearing was used for the initial evaluation of the force capability of the actuator. An added assumption in this case is that the curvature of the outer part of the pole pieces has negligible effects. The force exerted on the rotor by each pair of poles (i.e., by each one of the four horseshoe electromagnets) is

$$F_{rad} \approx \mu_0 \frac{N^2 i^2}{4t^2} S_t \cos\left(\frac{\pi}{8}\right) \quad , \tag{2}$$

where the nominal air gap is t = 0.5 mm. The resistance and the inductance of the electromagnets can be computed by the second and third equation (1). A maximum radial force of 160 N at 5 A with the nominal air gap of 0.5 mm is so computed.

This mathematical model does not allow us to study the effects of changes in the detailed design of the pole pieces, particularly where the fillets are concerned, and the possibility of the occurrence of local saturation of the material. A FEM simulation of the magnetic circuit was then undertaken with the aims of validating the simpler model and to gain a greater insight on the actual working of the actuator. The magnetostatic two-dimensional FEM model, built using ANSYS 4.4A code running on a Vax-Station 2000, includes 3198 4-node plane elements with a single degree of freedom per node (potential vector of the magnetic field), for a total of 2545 degrees of freedom. It takes into account the actual geometry of the cross section of the magnetic circuit and the magnetization curve of the soft-iron, including saturation. Being a plane model, it cannot take into account the end effects, which are at any rate assumed to be small and can be evaluated only at the cost of a very much more complex three-dimensional FEM model. An experimental validation was planned for this issue.

The model yields the value of the magnetic interaction force and the distribution of the magnetic field intensity H and the magnetic flux density B allowing us to verify the assumptions of uncoupling between the 4 electromagnets and to identify potential local saturation problems. The latter result is very useful to the end of optimizing the geometry of the magnetic circuit and particularly the fillet between the prismatic part of the poles and the pole shoes.

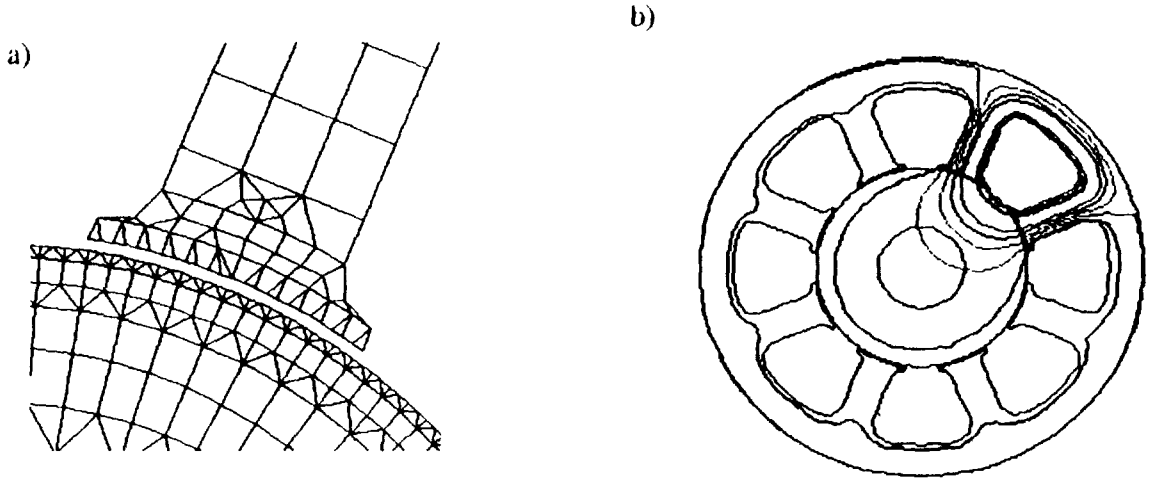

Figure 4. FEM model of the radial bearing. a) Particular of the mesh at the extremity of one pole piece. The elements simulating the air gap are not shown. b) Pattern of the magnetic field intensity H at $i = 5$ A and $t = 0.5$ mm.

Three numerical simulations were run: the first two with the rotor in the nominal position (air gap $t = 0.5$ mm) and values of the current of $i = 1$ A (within limits of linearity of the magnetic behaviour of the material) and $i = 5$ A, well into the saturation range of the material. For the highest value of the current, a further computation has been run with a larger value of the air gap, $t = 0.6$ mm, i.e. with the rotor in an off-centre position.

A particular of the FEM mesh is shown in Figure 4a. The pattern of the magnetic field intensity H obtained for the case of the higher current and rotor in the nominal position is shown in Figure 4b. The uncoupling between the electromagnets is clear, as the magnetic field is mainly confined in the zone adjacent to the working electromagnet. At this value of the current the magnetic circuit is partially saturated ($B = 1.4 - 1.5$ T). Enlargements of Figure 4b show that the distribution of the magnetic field in the pole shoes is not uniform and that saturation occurs mainly in the zone of the fillets. The value of the magnetic force is then lower in the case of the FEM than in that of the simpler model which neglects this effect (143 N against 160 N at 5 A with the nominal air gap of 0.50 mm).

Another interesting result is the fact that the magnetic field penetrates in the rotor deeper than the thickness of the soft iron laminations and interests the 39NiCrMo3 steel core. This effect can give way to eddy currents, with possible energy losses and heating of the shaft. The low value of the field in the core of the shaft leads to the suggestion that these effects are not strong and no modifications aimed at having a thinner shaft were planned at this stage.

The radial sensors are located in the same housing of the actuators. Initially Selet B18/5 OC inductive sensors were used but after the first tests it was clear that their performance was not adequate, particularly where the cutoff frequency is concerned; they were then substituted by Bently Nevada 3106 mod. 20886-01 inductive sensors. These last sensors cannot be exactly collocated with the actuators and in the present application the distance between the axes of the two elements is 52 mm; this can have an effect on the dynamic behaviour of the system and this issue was later studied in detail.

Also the emergency ball bearings are located in the same housings. A pair of deep groove Barden 104SST5CXO ball bearings were used, leaving a radial and axial clearance equal to half of the nominal air gap of the bearings (0.25 and 0.375 mm in radial and axial direction respectively).

Electric motor, shaft and base

The electric motor is a squirrel cage asynchronous motor. Its construction is similar to that of the radial bearings, with the difference being the squirrel cage in the rotor and the number of the slots (24) in the stator. The pattern of the windings is standard.

The shaft has been obtained from a single forging of 39NiCrMo3 steel UNI 7845, heat treated to a hardness of 43 HR_C at the surface (42 HR_C at the core). Its design incorporates a central zone on which a pulley or a flywheel can be fitted to experiment on the device. The rotors of the actuators and of the electric motor are directly shrink-fitted on the shaft. The measured inertial properties of the rotor assembly are mass 5.310 kg; moment of inertia about the rotation axis $1.8089\ 10^{-3}$ kg m^2 and transversal moment of inertia $1.1500\ 10^{-1}$ kg m^2.

The electromechanical parts are directly bolted on a light alloy base (anodized extruded bar of Al-MgSi0,5 UNI 3569-66). This solution allows a very simple interchangeability of the parts and the possibility of modifying the configuration of the device. The Selet B18/5 OC inductive axial sensor is directly bolted on it.

Control system, controller and power amplifier

A set of 5 equal SISO linear control systems has been designed, each one controlling a couple of electromagnets. No design difference in the controllers of the axial bearings or of the "vertical" or "horizontal" channels of the radial bearings has been introduced; however, as the control parameters can be adjusted by control handles on the front panel of the controller, the various controllers can have different settings.

The force-current characteristic of the electromagnets (equations 1 and 2 can be written in the synthetic form $F = K(i/t)^2$) is intrinsically nonlinear and must be linearized. Here the usual practice of superimposing a bias current to the control current is followed [11], even if provisions for attempting different strategies are included in the device and will be tested later.

Constant K can be either computed using equations (1) or (2), computed from results of finite element simulation, or measured experimentally. This approach does not include the saturation of the pole pieces, but this is not considered as a strong inconvenience, as linearization of the behaviour of the system is important only for values of the current which are low enough to prevent that phenomenon to occur. As shown in [4], [5], [11], the linearized expression of the force supplied by the pair of electromagnets connected to a single controller at varying control current i_c (i_o is the bias current) and displacement u from the nominal position is

$$F_{rad_{lin}} = -4K\frac{i_o}{c^2}i_c + 4K\frac{i_o^2}{c^3}u \tag{3}$$

where c is the clearance, which is assumed as constant as the linearization is performed about the centred position. The second term at the right hand side is linked with the unstable behaviour of the uncontrolled magnetic bearing.

A value of the bias current $i_0 = 0.45$ A was chosen as it allows to counteract the weight of the rotor in the "vertical" channels and insures a wide enough linear range without leading to a high power consumption (0.1 W per pair of electromagnets in the horizontal direction).

The problem of controlling the five axes of the rotor (a multivariable problem) has been reduced to the independent control of each axis by means of separate and identical controllers (a multiple monovariable problem). This approach is justified by the relative uncoupling of the machine (almost complete in the case of axial versus radial axes) and by the additional intrinsic uncoupling effect of feedback control. The independent axes solution is particularly advantageous in relation with the physical implementation of the control with analog active filters: the control of the five axis is then implemented by five identical boards carrying external potentiometers to adjust the single axis control parameters.

In order to design the control two simplified models of the rotor have been devised:

- 2 mode multivariable models obtained either by reducing the model on the actuator nodes (assuming collocated sensors) or by modal reduction; these models can describe rigid body modes only;
- single axis, i.e. monovariable, models obtained by structural analogy with a rigid body (Figure 5a) and with a flexible body (Figure 5b).

The first type of model has been used to assess stiffness and damping in terms of gains of a state space feedback control law obtained with standard pole-placement technique. The considered states being position and velocity, the control gains may be thought as a proportional and a derivative action directly on the position signal. For example, requiring the following pole shifting from unstable to stable and reasonably damped rigid modes

$$\begin{Bmatrix} -60.517 \\ +60.517 \\ -88.389 \\ +88.389 \end{Bmatrix} \rightarrow \begin{Bmatrix} -30+j300 \\ -30-j300 \\ -45+j380 \\ -45-j380 \end{Bmatrix} ,$$

(expressed in 1/s), the following gain position and velocity gain matrices are obtained

$$[K_p] = \begin{bmatrix} 3.757 & 1.218 \\ 1.332 & 2.935 \end{bmatrix} , \qquad [K_v] = \begin{bmatrix} 2.23710^{-3} & 7.34610^{-4} \\ 7.95710^{-4} & 1.79610^{-3} \end{bmatrix} .$$

The second type of model has been developed to take into account the flexural behavior of the rotor as "seen" by every position sensor and consequently fed back to the independent single axis controller. In this sense the damping action of the derivative term must be extended in order to cope with the flexural behavior even for sub-critical working velocities. The control loop of each axis is sketched in Figure 6.

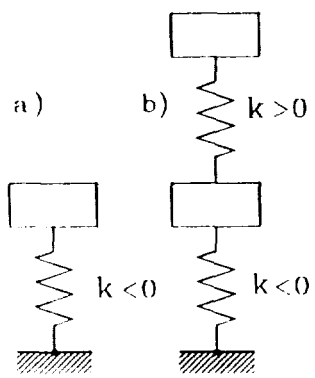

Figure 5. Single axis rigid body (a) and flexible body (b) model.

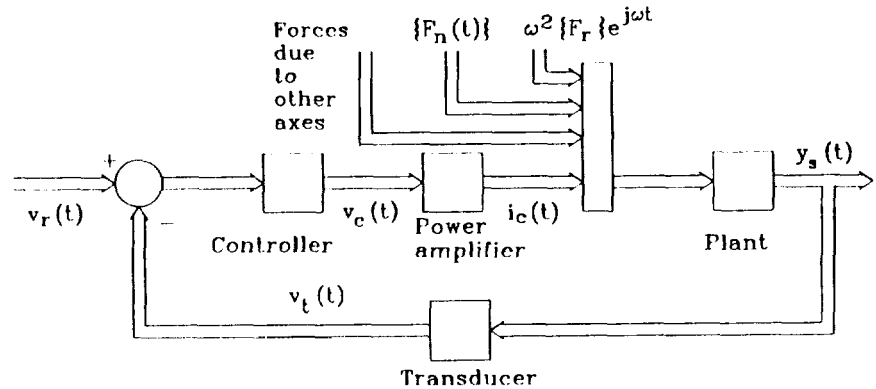

Figure 6. Single axis control loop.

Signal $r(t)$ is the position reference used to center the shaft with respect to the coil poles and emergency ball bearings. Since it remains unchanged during spindle operation the control problem is a pure regulation problem: to maintain the position in face of stationary and unbalance forces $\{F_n\}$ and $\omega^2\{F_r\}e^{j\omega t}$. Actually the controller has already been predisposed for a general two degrees of freedom control scheme with separate paths for sensor output and reference signals.

The basic structure of each axis' independent controller is the parallel of proportional, integrative and derivative command actions, that is a *PID* controller

$$v_c(t) = K_c\left(e(t) + \frac{1}{T_i s}\int_0^t e(\tau)d\tau + T_d\frac{d}{dt}v_i(t)\right) \quad , \tag{4}$$

where $v_c(t)$ is the controller output signal, $e(t) = v_r(t) - v_i(t)$ the error feedback signal, K_c the controller gain, T_i the integrative or reset time constant and T_d the derivative or prediction time constant. Including the causal pole in the derivative term on the error signal, the Laplace domain *PID* transfer function is

$$PID(s) = K_c\left(1 + \frac{1}{T_i s} + \frac{T_d s}{\tau_d s + 1}\right) \approx K_c\frac{1}{T_i}\frac{T_i s + 1}{s}\frac{T_d s + 1}{\tau_d s + 1} = PI(s)\,D(s) \quad . \tag{5}$$

The approximated expression holds if $T_i \gg T_d \gg \tau_d$ and can be interpreted as the series of a *PI* and phase lead filter.

The specifications assumed to design the controller may be summarized as follows:

- static stiffness greater than $0.5\ 10^6$ N/m;
- settling time to reach 90% of exact reference position, less than 5 s;
- reasonable damping in the frequency range covering rigid and flexural modes;
- attenuation of command action due to sensor high frequency disturbances.

The controller parameters obtained are then assumed as central value for the controller to be implemented circuitally: gain, $K_c = 3.0$, range $0.5 \div 5.5$; integrative time, $T_i = 5.0$ s, range $3.0 \div \infty$; and prediction time, $T_d = 6.3\ 10^{-4}$ s, range $1.0 \div 11.5\ 10^{-4}$. The causal pole has been placed in $\tau_d = 50\ 10^{-6}$ s. In order to improve compliance to the last piece of specification an additional filter may be added to the sensor output.

The electromagnet coils constitute a high inductance and low resistance load to the transconductance amplifier that conveys the levitation power to the shaft in accord with the controller output signal. The dissimilarity between the high voltage needed to change coil current and the low voltage needed to maintain it may result in an extremely low overall circuit efficiency with consequent dissipation problems. In order to increase the efficiency, the power section of the transconductance amplifier has been implemented with two Darlington pairs (TIP41C-BUV20) in parallel, one supplied with a low voltage to contribute the constant equilibrium and superposition currents acting on the resistive part of the load, and the other with a high voltage to output the high operating voltage needed to overpower the coil back-electromotive force.

The above described power section with roughly unit signal gain is then inserted in a high gain current feedback loop made by a high voltage operational amplifier (LM343) and an amplified shunt resistor, forcing unitary feedback. An adjustable overload limit circuit has also been added on the feedback path. A gain of 330k/10k moves the power amplifier cutoff frequency up to 812 Hz with almost unitary overall gain (1.023).

Axial bearing

The experimental testing on the axial bearing was based on the measurement of the magnetic interaction force between the stator and the rotor for different values of the current and different positions of the rotor. The inductance and the resistance of the electromagnets were also measured.

The force measurements were performed by fixing the housing of the bearing on a table which can be displaced along the axial and two radial directions by means of micrometric slides. The rotor disc was fixed on a shaft connected to a load cell. Only one electromagnet was powered and consequently only the attractive force in one direction was measured. The instrumentation used allowed us to obtain an accuracy of 0.01 mm for displacements (dial gauge), 0.03 N for forces (load cell - multimeter), 0.01 A for currents (stabilized current supply) and 0.1 mΩ for resistances (digital multimeter). The variation ranges of the values of the test parameters in the different tests were 0.75-1.5 mm (step 0.25 mm) for the air gap t and 0-7 A (step 0.5 A) for the current i. Each test was performed by repeating the measuring cycle 3 times for a total of 360 force measurements.

The force-current curves at constant air gap and the force-distance curves at constant current are reported in Figure 7. The experimental points are plotted together with least-squares fit. The exponents of the least square curves differ from the values 2 and -2 predicted by equation (1) and some difference between the curves obtained with increasing current (air gap) and those obtained with decreasing current (air gap) is evident. There is no doubt that the hysteresis effect is linked with the use of steel for the magnetic circuit instead of soft iron, while the displacement of the curves from the theoretical ones is due to saturation (force-current relationship) and to the finite value of the permeability of iron (force-distance relationship). A comparison between numerical and experimental results is shown in Table I and Table II.

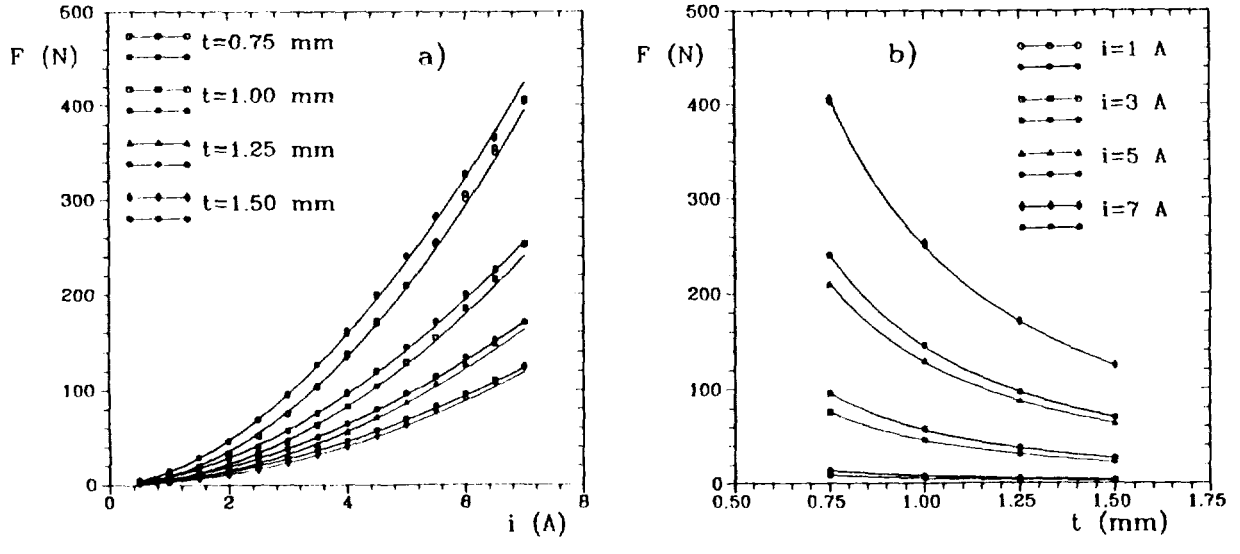

Figure 7. Results of the force tests for the axial bearing. a) Force versus current at constant distance. Experimental points and interpolating expression $F = ai^b$ with b = 1.90 for increasing current and b = 1.75 for decreasing current. b) Force versus air gap at constant current. Experimental points and interpolating expression $F = at^b$ with b = -1.71 for increasing air gap and b = -1.79 for decreasing air gap.

Table I. Measured and Computed Electrical Characteristics of the Axial Bearing

R [Ω]			L [mH]		
Computed	Exp. coil 1	Exp. coil 2	Computed	Exp. coil 1	Exp. coil 2
0.395	0.433	0.431	13.96	14.12	14.04

Table II. Measured and Computed Values of the Force of the Axial Bearing for Two Values of the Current and Nominal Air Gap t = 0.75 mm. (*) Eq. (2); (**) As Equation (2), but Without Neglecting the Reluctance of the Pole Pieces

	i = 1.00 A		i = 5.00 A	
	F [N]	error	F [N]	error
Experimental	8.8	---	210.1	---
Computed (*)	9.7	10.2 %	243.3	15.8 %
Computed (**)	8.9	1.1 %	223.6	6.4 %

Radial bearings

Two different pairs of radial actuators were built and tested, the difference being mainly in the number of conductors. Only the results obtained on the second prototype, whose performance proved to be better than that of the first one, are here reported.

The test rig and instrumentation used are the same seen for the axial bearing, and are the same for the test procedures. The variation ranges of the values of the test parameters in the different tests were 0.3-0.8 mm (step 0.1 mm) for the air gap t, 0-4 A (step 0.25 A) and 4-8 A (step 0.5 A) for the current i. Each test was performed by repeating the measuring cycle 3 times for a total of 612 force measurements.

The force-current curves at constant air gap and the force-distance curves at constant current are reported in Figure 8. Only tests conducted with currents up to 4 A are reported. The experimental points are plotted together with least-squares curves. In this case only negligible hysteresis effects have been found, owing to the use of soft iron for the pole pieces; no distinction between the curves obtained with increasing current (air gap) and those obtained with decreasing current (air gap) has been made. The exponent of the least square force versus current curve is very close to 2, as predicted by equation (2): in the present current range no noticeable saturation takes place. On the contrary the exponent of the least square force versus air gap curve is far from the value -2 predicted by the simplified model. A comparison between numerical and experimental results is shown in Table III and Table IV.

Curves similar to those of Figure 8a but also for higher values of the current are plotted in Figure 9. Some saturation at high current and low air gap is clearly present and a 4-th degree polynomial has been used for the least-square fit. The curves for the smallest air gap have been limited to 4 A to avoid overloading of the load cell.

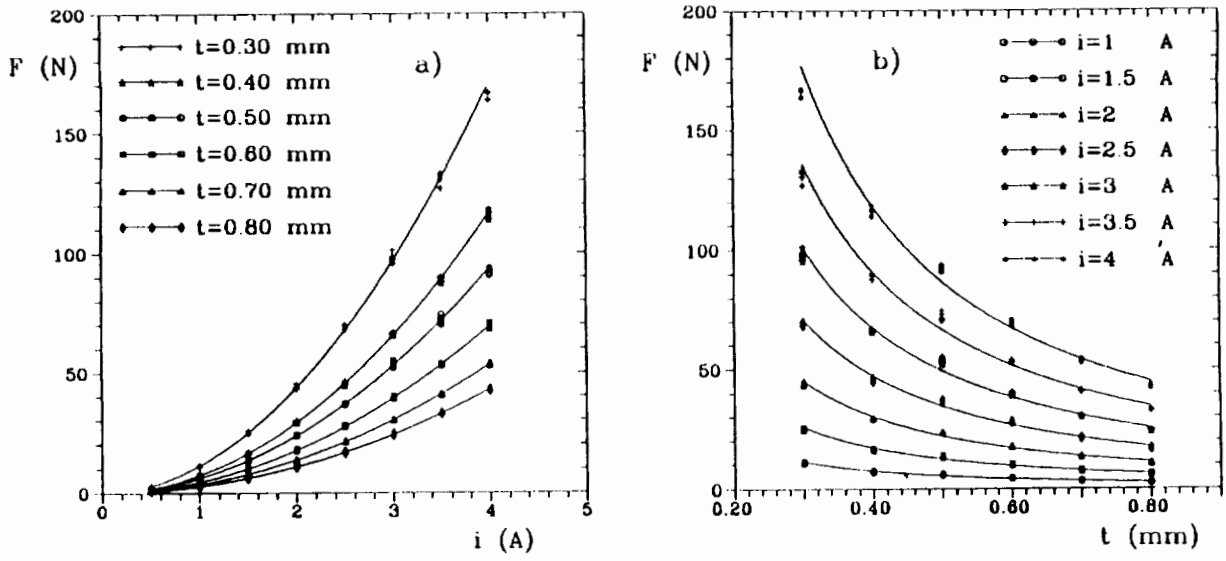

Figure 8. Results of the force tests for the radial bearing. a) Force versus current at constant distance. Experimental points and interpolating expression $F = ai^b$ with b = 1.99. b) Force versus air gap at constant current. Experimental points and interpolating expression $F = at^b$ with b = -1.41.

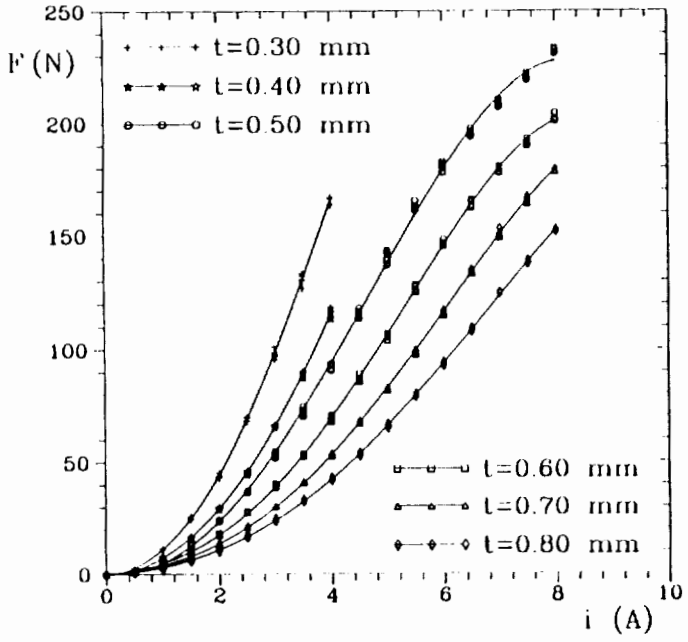

Figure 9. As Figure 8a, but for higher values of the current. Fourth degree polynomial least-square fit.

Further experimental tests were conducted to verify the linearization strategy mentioned above. The tests were conducted by superimposing a fixed bias current i_o to the control current i_c in a pair of opposite electromagnets and measuring the force with the rotor in the nominal (centred) position. The variation ranges of the values of the test parameters in the different tests were 1-2.5 A (step 0.5 A) for the bias current i_o, 0-i_o A (step 0.25 A) and i_o-8 A (step 0.5 A) for the control current i_c. Each test was performed by repeating the measuring cycle 3 times for a total of 432 force measurements. The results are shown in Figure 10a.

Table III. Measured and Computed Electrical Characteristics of the Radial Bearings

R [Ω]			L [mH]		
Computed	Exp. rad. 1	Exp. rad. 2	Computed	Exp. rad. 1	Exp. rad. 2
0.205	0.225	0.224	6.75	6.53	6.49

Table IV. Measured and Computed Values of the Force of the Radial Bearings for Two Values of the Current and Two Values of the Air Gap

	t = 0.50 mm				t = 0.60 mm	
	i = 1.00 A		i = 5.00 A		i = 5.00 A	
	F [N]	error	F [N]	error	F [N]	error
Experimental	5.9	---	140.6	---	105.8	---
Equation (4)	6.3	6.8 %	160.0	13.8 %	108.3	2.4 %
FEM	5.8	1.7 %	143.3	1.9 %	104.8	0.9 %

By superimposing the curves obtained from the previous tests it is possible to compute from experimental results the value of constant K to be introduced into equation (2). A value K = 1.525 N mm^2/ A^2 was then used in the further parts of the work (Figure 10b).

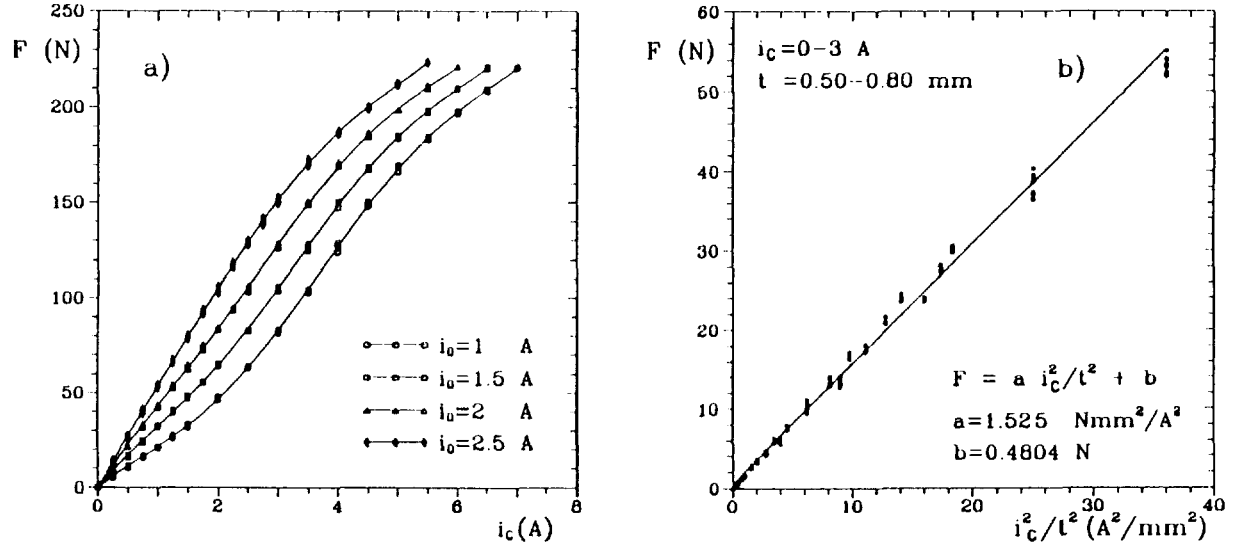

Figure 10. a) Results of the linearization tests for the radial bearing. Force versus control current at constant bias current. b) Force exerted by a pair of electromagnets versus parameter $(i/t)^2$, obtained by adding the experimental values of the previous tests.

EXPERIMENTAL TESTING OF THE SYSTEMS

Before running the system, the natural frequencies of the suspended rotor were measured by exciting the system with an instrumented hammer and measuring the acceleration at midspan. The first 3 values are compared with the numerical results in [11].

A series of spin tests have been performed up to a speed of 21000 rpm, which is lower than the critical speed related to the first deformation mode (third critical speed), expected at 25780 rpm. The amplitude of the orbit at the sensor location was recorded as a function of the spin speed during free spin-down from the maximum speed. The amplitude of the orbit has been obtained directly from the output of the sensors, using their gains. The synchronous component of the amplitude in horizontal direction obtained from a frequency analyzer is plotted in Figure 11.

The maximum amplitude of about 54 μm is reached during the crossing of the two rigid-body critical speeds, while the amplitude in the supercritical range is lower than about 15 μm. The corresponding values measured by an accelerometer located on the stator are of 13 μm and 0.2 μm respectively. The latter accounts for the extremely smooth running of the machine.

The measured critical speeds at 3300 and 4020 rpm are close to the computed values of 2990 and 3880 rpm.

Several tests aimed to verify the stability of the system were performed introducing disturbances both in form of impulsive loads on the stator and added unbalances on the rotor. In all cases the system proved to be able to maintain stable working conditions and reject disturbances.

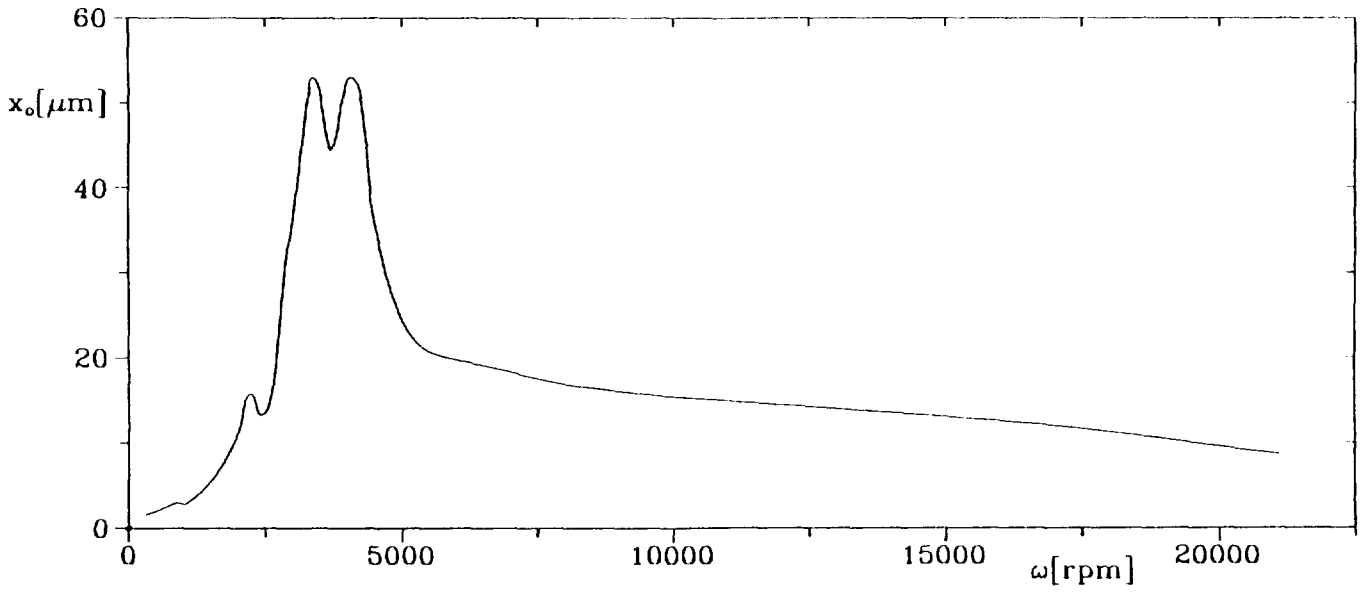

Figure 11. Results of a spin-down test: amplitude of the synchronous component of the displacement at one sensor location in horizontal direction versus spin speed.

CONCLUSIONS

The electric spindle supported by a five-active axes magnetic suspension built at the Department of Mechanics of Politecnico di Torino has been described in detail.

The machine has been tested thoroughly in the speed range up to the third critical speed, corresponding to the first deformation mode of the shaft. In this speed range it proved to be capable of stable operation even in presence of disturbances and to be extremely quiet and vibration free. Further tests aimed to exceed the third critical speed are planned; as numerical simulation shows that the amplitude in this condition is not small enough [11], suitable modifications to the controller are planned.

The device is now used as an experimental rig and as a teaching support.

A very interesting feature of the whole project is its low cost, which can effectively open new application areas to the active magnetic suspension technology.

REFERENCES

1. Genta, G.; Mazzocchetti, L.; and Rava, E.: Magnetic Suspension for a Turbomolecular Pump. 2nd. International Symp. on Magnetic Bearings, Tokyo, July 1990, pp. 65-72.
2. Genta, G.; Delprete, C.; Tonoli, A.; Rava, E.; and Mazzocchetti, L.: Study of the Geometry of a Passive Radial Magnetic Bearing for Application to a Turbomolecular Pump. MAG'92 Magnetic Drivers and Dry Gas Seals Conference & Exhibition, Alexandria, Virginia, July 1992, pp. 61-70.
3. Delprete, C.; Genta, G.; Mazzocchetti, L.; Rava, E.; Ricca, A.; Ripamonti, G.; Santini, L.; Tonoli, A.; Varesi, A.; and Zannella, S.: High Speed Asynchronous Motor with High T_c Superconducting Bearings. 3rd. International Symp. on Magnetic Bearings, Alexandria, Virginia, July 1992, pp. 287-296.
4. Schweitzer, G.; and Lange, R.: Characteristics of a Magnetic Rotor Bearing for Active Vibration Control. 1st. International Conf. on Vibrations in Rotating Machinery, Cambridge, September 1976, IMechE C239/76, pp. 1-6.
5. Schweitzer, G.: *Magnetic Bearings*, Lecture Course "Rotordynamics - 2", CISM (Centre Int. Sciences Mech.), Udine, October 1985.
6. Gondhalekar, V.; and Holmes, R.: Design of a Radial Electromagnetic Bearing for the Vibration Control of a Supercritical Shaft. Proc. IMechE 198C(16), 1984, pp. 235-242.
7. Imlach, J.; Allaire, P.E.; Humphris, R.R.; and Barrett, L.E.: Magnetic Bearing Design Optimization. Proc. IMechE Vibrations in Rotating Machinery, Edinburgh, September 1988, pp. 53-60.
8. Jeyaseelan, M.; Anand, D.K.; and Kirk, J.A.: A CAD Approach to Magnetic Bearing Design. Proc. 23nd IECEC Intersoc. Energy Conversion Eng. Conference, Denver, Colorado, July 1988, vol. 2, pp. 37-42.
9. Maslen, E.H.; Allaire, P.E.; and Scott, M.A.: Magnetic Bearing Design for a High Speed Rotor. 1st International Symp. on Magnetic Bearing, Zurich, June 1988, pp. 137-148.
10. Walowit, J.A.; and Pinkus, O.: Analytical and Experimental Investigation of Magnetic Support Systems. Part I: Analysis - Part II: Experimental Investigation. Trans. ASME J. Lubr. Tech., 1982, vol. 104, pp. 418-437.
11. Genta, G.; Delprete, C.; and Carabelli, S.: Active Magnetic Bearing Control Loop Modeling for a Finite Element Rotordynamics Code. 2nd. International Symp. on Magnetic Suspension Technology, NASA CP3247, Seattle, Washington, August 1993.